ELSEVIER

19 December 1997

Chemical Physics Letters 281 (1997) 10–19

CHEMICAL PHYSICS LETTERS

Ultrafast electron diffraction: structures in dissociation dynamics of $Fe(CO)_5$

H. Ihee, J. Cao, A.H. Zewail

Arthur Amos Noyes Laboratory of Chemical Physics, California Institute of Technology, Pasadena, CA 91125, USA

Received 15 September 1997; in final form 6 October 1997

Abstract

We report on the application of ultrafast electron diffraction (UED) to the study of complex molecular reactions, the dissociation of $Fe(CO)_5$. Snapshots of the diffraction images were recorded at different reaction times. The reaction was initiated by a femtosecond pulse and clocked accurately within 2 ps. The dissociation is complete in less than 10 ps and we identify major product distributions and structures; $Fe(CO)_2$, Fe(CO) and Fe in the branching ratio of ca. 2:5:5. The C–O distance becomes longer, relative to that of $Fe(CO)_5$, suggesting a non-systematic weaker C–O bond in $Fe(CO)_2$ and Fe(CO) fragments. The temporal diffraction-difference method greatly enhances the ability of recording structural changes in UED. © 1997 Elsevier Science B.V.

1. Introduction

In continuation of our efforts [1,2], we report here on the extension of the ultrafast electron diffraction (UED) technique to the study of complex molecular reactions, namely the dissociation reaction of $Fe(CO)_5$. Clocking (time zero) of the reaction in the gas phase was determined accurately within 2 ps. The reaction was initiated by a femtosecond (fs) laser pulse (310 nm and two photons), and snapshots of the diffraction images were recorded at different delay times. The methodology of recording the diffraction *before* and *after* time zero (*diffraction difference*) makes it possible to observe structural changes with calibration of all parameters except for the temporal evolution of the reaction itself. After 10 ps and up to delay times of 270 ps, we observed no structural change indicating that the dissociation of $Fe(CO)_5$ occurs in less than 10 ps. On this ps time scale, the final major products were found to be $Fe(CO)_2$, FeCO and Fe with a branching ratio of ca. 2:5:5. Preliminary analysis provides the Fe–C and C–O bond distances of transient structures of $Fe(CO)_2$ and FeCO.

Gas-phase diffraction of molecules in their ground state has been a powerful tool over the past fifty years [3]. Diffraction methods, generally utilizing X-rays or electrons, are direct approaches for determining complex structures and progress in such studies of structural changes continues in several laboratories [1,2,4–9]. Our focus here and before has been on gas-phase UED. For gas-phase UED to succeed, major challenges must be surmounted because of the very low number densities of gas samples, the absence of long-range order in crystals which enhances coherent interference, and the challenging task of determining in situ the zero of time when diffraction changes are on the ps and sub-ps time scale.

In order to probe ps and sub-ps changes, three basic capabilities were incorporated into our appara-

PII S0009-2614(97)01167-6

tus: (1) accurate clocking of the reaction, (2) measurement of the electron pulsewidth, and (3) detection of single electrons (necessary to reduce the electron flux and minimize space–charge broadening). A schematic of the apparatus is shown in Fig. 1. In previous work in this laboratory, we studied halomethanes and haloethanes because of their strong scattering and high absorption cross sections. For CH_2I_2, the changes due to C–I bond breakage were successfully detected, after CH_2I_2 dissociation into CH_2I, with 15 ps time resolution. $Fe(CO)_5$ represents additional challenges because of its complexity and the multiple reaction paths.

The chemistry of transition metal carbonyls is rich [10,11]. After absorbing ultraviolet photons, they dissociate into reactive unsaturated carbonyls, which are known to catalyze a variety of interesting reactions [12,13]. Over the past decades, the photochemistry of coordinately unsaturated species has been the subject of studies of increasing depth and detail. Of particular interest are the reaction pathways, the binding energies of successive CO ligands, and the structures of the unsaturated species.

Much of the gas-phase photochemistry work on metal carbonyls has been devoted to $Fe(CO)_5$ and its unsaturated radicals. $Fe(CO)_5$ is known to absorb strongly in the ultraviolet starting at $\sim$ 350 nm (3.5 eV) [14,15]. The spectrum is rather featureless and thought to be dominated by ligand field d–d transitions at low energies and metal-to-ligand charge transfer transitions at high energies. The complete fragmentation of $Fe(CO)_5$ requires about 6.1 eV [16]

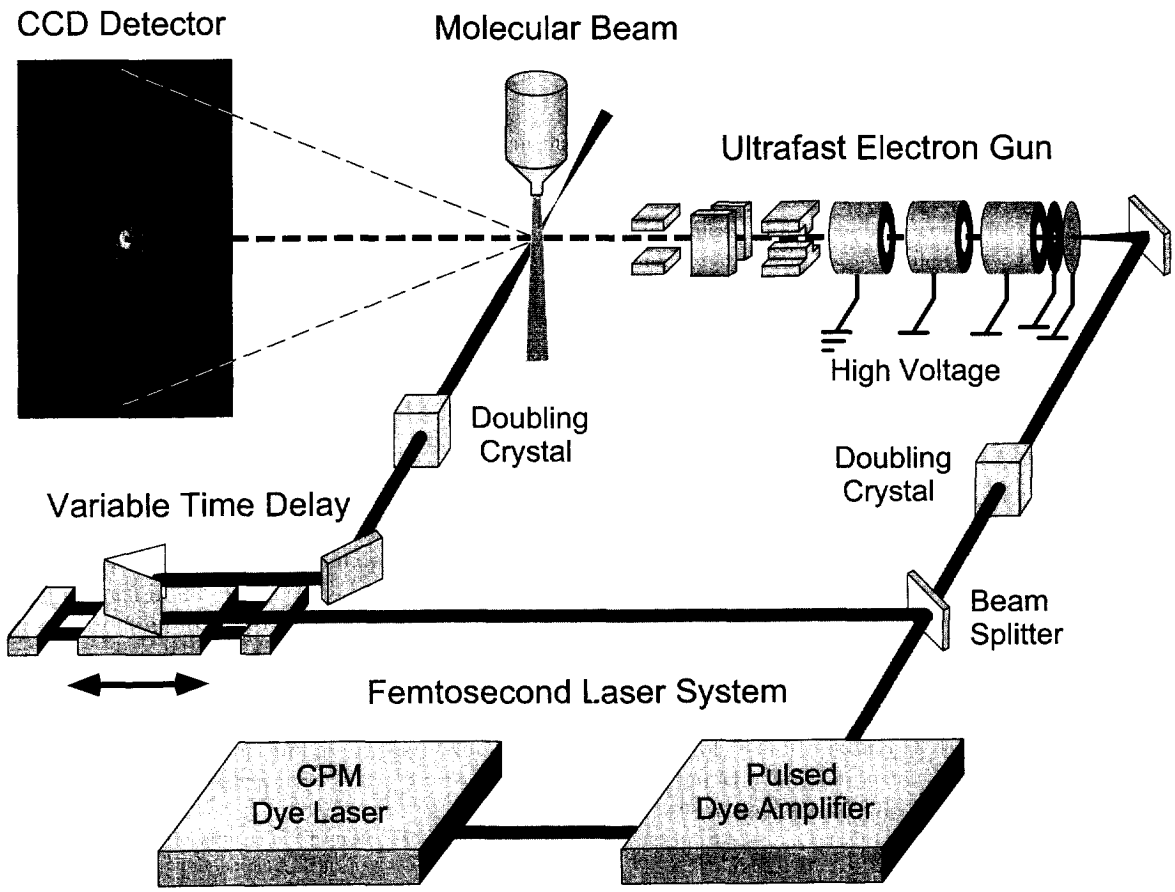

Fig. 1. A schematic of experimental apparatus for ultrafast electron diffraction (UED) in a molecular beam arrangement.

and the successive CO binding energies were reported to be ca. 2.0, 0.5, 1.5, 1 and 1 eV, respectively [17–20].

Fig. 2 presents structures of $Fe(CO)_5$ and its unsaturated fragments. The ground state of $Fe(CO)_5$ has a D_{3h} structural symmetry [18,21,22]. After losing one CO ligand, $Fe(CO)_4$ develops a structure of a Jahn–Teller distorted tetrahedron with C_{2v} symmetry [23]. The further dissociation produces $Fe(CO)_3$ of C_{3v} symmetry with an out-of-plane bend angle θ of 21° [23,24]. Both $Fe(CO)_2$ and FeCO have linear structures due to the Fe–C σ-bond and C–O π-bond [22,25]. However, except for the structure of the $Fe(CO)_5$ parent molecule, which was determined by gas-phase electron diffraction (GED) [21], the internuclear distances of its unsaturated fragments have not been precisely determined.

Several research groups have investigated the mechanism and the dependence of the reaction on excitation wavelength. Of particular interest is the issue of whether the dissociation occurs in a concerted or sequential manner when multiple CO fragments depart. Using chemical trapping methods [14,26], the distribution of $Fe(CO)_n$ ($n = 2, 3, 4$) resulting from one-photon absorption at 193, 248 and 352 nm was measured. It was shown that more CO ligands are lost as the laser photon energy increases, proposing a photodissociation process in which the CO ligands are lost sequentially. Several groups have examined this system and, in general, gave support to the mechanism of sequential CO liberation [27–30], although there are some differences as discussed below.

The first femtosecond study of the dissociation reactions of metal carbonyls in the gas phase was carried out on $Mn_2(CO)_{10}$ using fs-resolved mass spectrometry [31]. In these experiments, the temporal dynamics for both metal–metal and metal–ligand bond cleavage, occurring on a time scale of hundreds of femtoseconds, were identified. Very recently, the femtosecond dissociation dynamics of $Fe(CO)_5$ were studied by Bañares et al. [32]. $Fe(CO)_5$ was excited with two-photon absorption of 400 nm laser and transient mass spectra of each intermediate species were recorded using an 800 nm probe laser. Again, the time scale of dissociation was observed to be a few hundred femtoseconds. In contrast to previous one-photon studies which support a stepwise elimination of ligands, the authors suggested that Fe(CO) is formed in a concerted manner from $Fe(CO)_5$, and further dissociated into Fe. Our UED results are consistent with ultrafast dissociation dynamics and now elucidate major transient structures and channels.

2. Experimental

2.1. UED apparatus

The UED experiments on $Fe(CO)_5$ were performed in the second-generation apparatus developed

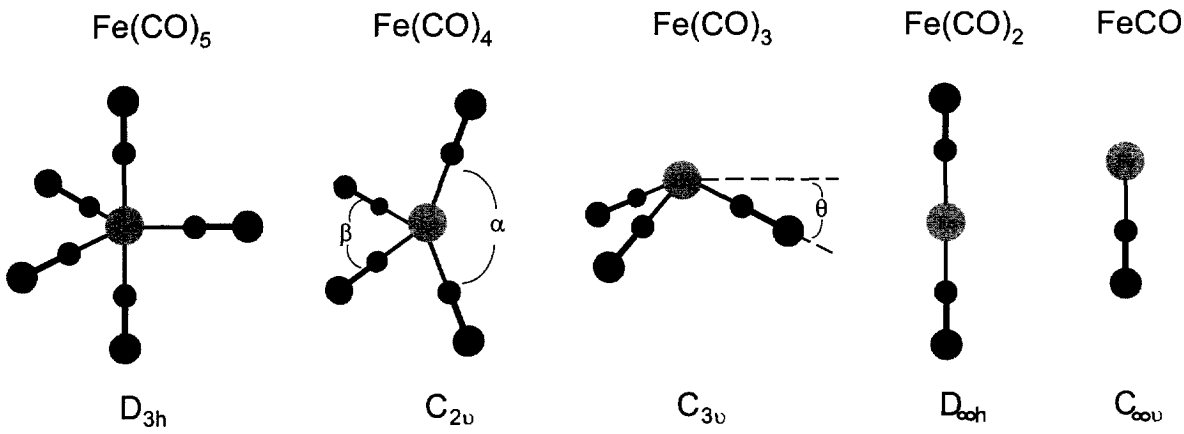

Fig. 2. Structures of $Fe(CO)_5$ and its unsaturated fragments of the dissociation reaction. The angles $\alpha = 145°$, $\beta = 120°$ [23], and $\theta = 21°$ [23,24].

in this laboratory, as described in greater detail elsewhere [1]. Briefly, it is composed of a femtosecond laser, a picosecond electron gun, a free-jet expansion sample source, and a two-dimensional single electron detection system (Fig. 1). Femtosecond laser pulses from a colliding-pulse mode-locked ring dye laser were amplified in a four-stage pulsed dye amplifier pumped by a Nd:YAG laser at 30 Hz. The amplified pulses (620 nm, 2–3 mJ/pulse, 30 Hz, ~ 300 fs pulse width) were then split (with a beam splitter) into two beams. The clocking laser pulse (95%) was first frequency-doubled with a KDP crystal (250 μJ at 310 nm), then directed and focused on the scattering gas sample beneath the needle of the free-jet expansion source.

To generate the electron pulse, the remaining 5%, also doubled, was focused onto a back-illuminated photocathode in the electron gun compartment. The ultrashort electron pulse was then accelerated to 18.8 keV (de Broglie wavelength is 0.088 Å) and focused onto the scattering volume. The two-dimensional diffraction images at a certain delay time were recorded in a charge-coupled device (CCD) at the end of a phosphor scintillator/fiber optic/image intensifier chain in the detection chamber. Time delays between the fs laser pulse and the ps electron pulse were controlled by a computer-driven translational stage.

2.2. Clocking and time resolution

The electron pulse, the laser pulse and the molecular beam were arranged in a cross-beam geometry, and the alignment of the three beams was controlled to within 10 μm accuracy. The camera length was measured to be 102.7 mm. For our current setup, the time resolution is mostly determined by the electron pulse width. With an electron flux of $\sim 10^4$ electrons per pulse in our experiment, the corresponding temporal width is 10 ps [1]. The total temporal resolution, including the contributions from pump laser pulse width (0.3 ps) and group velocity mismatch effect [1,2], is less than 12 ps. After we established in situ the time zero, by the lensing approach [1], to be within ±2 ps accuracy, we then obtained the time-resolved data at −20, +10, +40, +70 and +270 ps delay times.

Care was taken to purify the scattering sample of $Fe(CO)_5$ (Aldrich 98%). The sample was purified through vacuum distillation and then transferred into a sample cell under vacuum. After connection to the diffraction chamber, the sample was further purified by three freeze-and-thaw cycles to remove the residual impurities. The final sample purity was estimated to be better than 99%. In order to increase the density in the scattering volume, the sample cell, the gas line and the nozzle were heated to 38, 65 and 68°C, respectively. The gas pressure in the scattering chamber during the experiment was $\sim 4 \times 10^{-4}$ Torr. Clocking measurements and streaking of electrons (for pulse width measurement) were made in situ inside the molecular beam apparatus, where the diffraction changes with time were recorded.

3. Methodology and data analysis

At each delay time, a series of over 55 two-dimensional diffraction images (130 second average exposure time for each image) were recorded with the CCD detector. To extract the experimental total scattering intensity curve, $I_{Tot}(s)$, and the experimental modified molecular scattering function, $sM(s)$, we followed a detailed procedure of data analysis [1,2] similar to that of conventional gas-phase electron diffraction (GED) [3]. First, the center pixel coordinates (undiffracted electron beam spot) and the background offset (CCD dark noise) of each image were determined. With this information, the diffraction intensity as a function of pixel distance from the center, I(pix), was calculated by summing the total intensity counts at a specific pixel radius from the center and dividing the number of contributing pixels for each diffraction image. This conversion of the two-dimensional image to a one-dimensional intensity distribution imitates the effects of the radial microdensitometer used in the conventional GED. Finally, the experimental total scattering intensity curve $I_{Tot}(s)$ was obtained by further averaging all the I(pix) at each delay time and through the conversion of pixel number to momentum transfer s [2].

The experimental total intensity curve is a sum of the molecular scattering, $I_m(s)$ and the background intensity profile, $I_{Back}(s)$:

$$I_{Tot}(s) = I_m(s) + I_{Back}(s). \quad (1)$$

$I_m(s)$ is composed of interference terms from all atom–atom pairs, which contains molecular structural information. I_{Back} contains the contributions from atomic scattering, inelastic scattering, and other experimental background. Since the total scattering intensity decreases as the fifth power of s, a graph of the experimental modified molecular scattering intensity, $sM(s)$, is often plotted instead of $I_m(s)$ to bring out the oscillatory behavior at the higher values of s. The modified molecular scattering intensity is calculated accordingly [3,33]:

$$sM(s) = s\frac{I_{Tot}(s) - I_{Back}(s)}{|f_a||f_b|}, \qquad (2)$$

where f_a and f_b are atomic scattering amplitudes. The corresponding radial distribution curve, which provides the relative density of internuclear distances in a molecule, is then transformed from the $sM(s)$ curves using the standard GED equation:

$$f(r) = \int_0^{s_{max}} sM(s)\sin(sr)\exp(-ks^2)\,ds, \qquad (3)$$

where the constant k is a damping coefficient included for the limited s range ($k = 0.02$ Å^2 in our data analysis). The molecular structural parameters can be determined by fitting a structural model to the experimental modified molecular scattering intensity, $sM(s)$. With the high electron flux (on the order of microamperes), internuclear separations can usually be determined with a precision of 0.001 Å [3]; see Section 4.

The accuracy in UED has been so far (~ 0.05 Å) less than that of conventional GED because of the demand on time resolution. The electron flux must be kept very low (less than 100 femtoamperes) to maintain ultrafast temporal resolution; in conventional GED, the corresponding value is ~ 0.1 microampere. Thus, the signal-to-noise ratio is not yet optimum. In most cases, the fraction of excited molecules is less than 20% and not all the excited parent molecules are dissociated. Furthermore, the scattering intensity of a reaction fragment may be weaker than that of the parent and, therefore, they contribute less to the total scattering intensity than parent molecules.

To overcome these difficulties, a new *diffraction-difference* approach, capable of identifying the structure of each of the products, was introduced in this laboratory for UED. In principle, this method brings out the changes induced by the initiating laser in the difference-curve relative to the reference established before the initiation. In our experiment, since time zero was unambiguously determined within 2 ps and the experimental temporal resolution was less than 12 ps, the data at -20 ps established the reference which was not perturbed by the initiating laser [1]. The difference total intensity data, ΔI_{Tot}, at each positive delay-time point, was obtained by subtracting the I_{Tot} at -20 ps; ΔI_{Tot} was used instead of I_{Tot} for the analysis of transient structural changes. This diffraction-difference approach has several advantages. First, atomic scattering is a common contribution regardless of time and fragmentation and, therefore, it can be removed systematically by subtracting the -20 ps data from each positive time point. Second, any intrinsic systematic error of the detection system will be eliminated or greatly reduced after subtraction. Third, the diffraction-difference curve reflects the equally important contributions of the parent and products ($-1{:}1$), in contrast to the original raw data which contains a relatively small fraction of products and majority of parent. Therefore, the significance of the product contribution is dramatically enhanced in ΔI_{Tot}.

Theoretically, difference total intensity ΔI_{Tot} should be the same as the difference molecular scattering intensity (ΔI_m) and free from any background. This is because the background intensity should not change before and after time zero (see Eq. (1)). However, a small residual background was detected in our experimental ΔI_{Tot}. The origin of this residual background is tentatively assigned to the unique scattering effect of positive ions generated by a strong excitation laser through multiphoton ionization. Further investigation of this effect is in progress. The determination of the fraction and structural parameters of each fragment, for a given difference total intensity curve, ΔI_{Tot}, was made using a home-developed computer software in an iterative manner similar to that used in conventional GED [34,35]. Starting from an assumed product distribution and the structural parameters for each species, the software first fitted the residual background with the experimental ΔI_{Tot} values at the zero points of

theoretical $\Delta I_m(s)$. Then the experimental $\Delta sM(s)$ and $\Delta f(r)$ were obtained with the background-free ΔI_{Tot} through Eqs. (2) and (3). They were further compared with the theoretical $\Delta sM(s)$ and $\Delta f(r)$ to evaluate the goodness of the fit. This procedure was repeated until the best least-square fit between theoretical and experimental $\Delta sM(s)$ curves was reached [34,35].

4. Results and discussion

Fig. 3 shows the experimental $sM(s)$ and $f(r)$ curves at -20 ps and the difference $\Delta sM(s)$ and $\Delta f(r)$ curves at different delay times relative to the data of $Fe(CO)_5$ at -20 ps. The theoretical $sM(s)$ and $f(r)$, derived with the structural parameters from static gas-phase electron diffraction study [21], are also imposed on the -20 ps data for comparison. From the fit of our experimental ground state diffraction data (-20 ps), we obtained the following distances: 1.81 Å, 1.82 Å and 1.15 Å, for the Fe–C(axial), Fe–C(equatorial) and C–O, which are in good agreement with literature values (1.807 Å, 1.827 Å and 1.152 Å). Agreement between theory and experiment is very good considering the extremely low flux of our ps electron pulse. Note that our k value is 0.02 Å^2 and our $f(r)$, which displays the prominent and expected peaks, is of less resolution than that reported in the literature with smaller

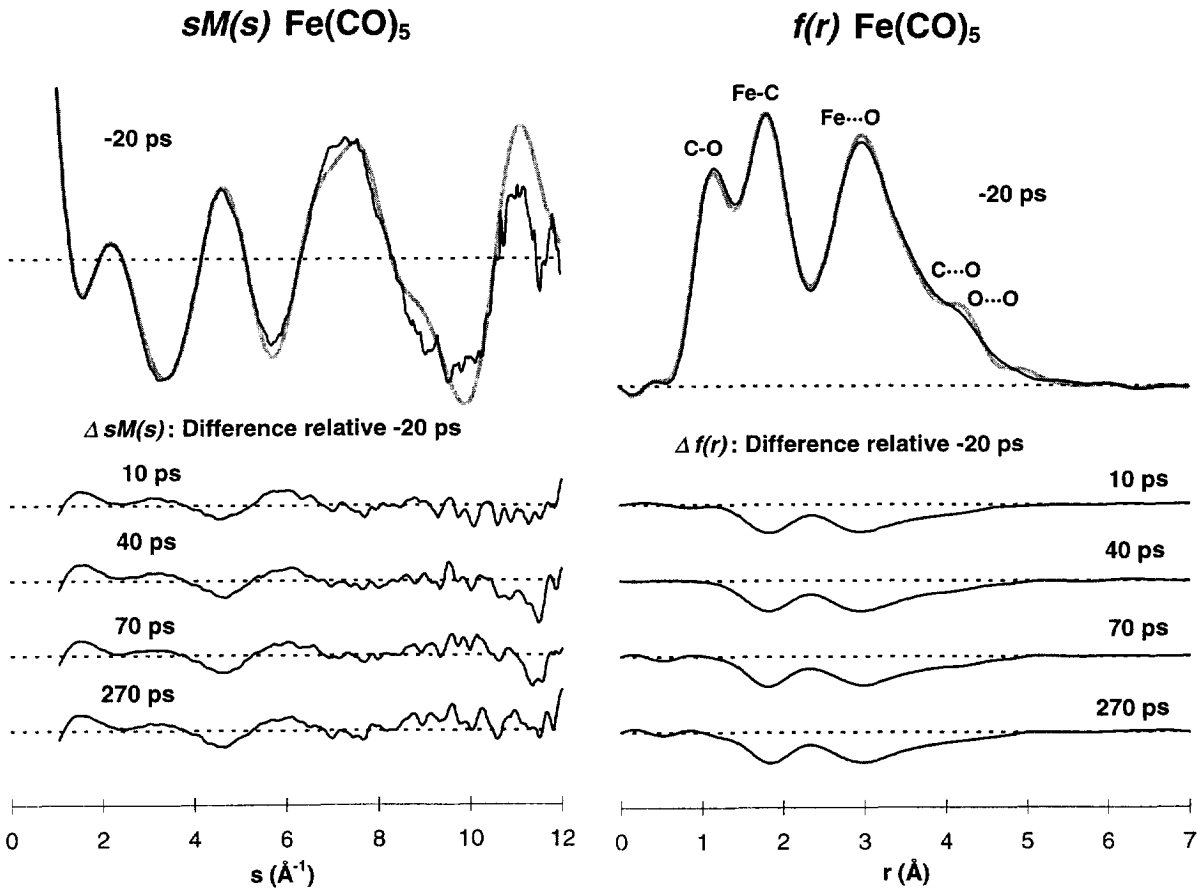

Fig. 3. UED of $Fe(CO)_5$ reaction. Experimental modified molecular scattering curves (left) and radial distribution curves (right) taken with the 10 ps electron diffraction pulses. The delay time between the fs laser pulse and the ps electron pulse are shown. Shaded lines represent the theoretical calculations with structural parameters from ground-state electron diffraction data [21]; we also fitted our experimental results to obtain the structure and found them to be in good agreement; see text.

values of k ranging from 0.01 to 0.0025 Å^2. As shown in Fig. 3, the difference curves of each positive time point are identical within our experimental error.

The absence of temporal evolution after 10 ps indicates that the whole fragmentation process takes place in less than 10 ps. This is consistent with the recent study on $Fe(CO)_5$ using two photons of 400 nm pump and 800 nm probe fs lasers [33], where they found that the final fragments were formed within 500 fs. The two main peaks centered at 1.82 Å and 2.98 Å in the difference curves indicate the depletion of the Fe–C and Fe $\cdots$ O internuclear contribution after the $Fe(CO)_5$ parent molecules dissociated into $Fe(CO)_x$ ($x = 4, 3, 2, 1, 0$). The shoulder beyond 3.5 Å is due to the reduction of other internuclear contributions, C $\cdots$ O and O $\cdots$ O. *Note that the peak for the C–O bond at 1.15 Å is absent in the $\Delta f(r)$*, indicating the successful methodology outlined in the previous section. This is because the number of CO moieties is conserved in the course of the reaction, before and after time zero (C–O distance in $Fe(CO)_5$ is 1.15 Å and that of free CO is 1.13 Å).

Having five carbonyl moieties, a $Fe(CO)_5$ molecule can dissociate into five different products depending on the excitation wavelength. Direct and indirect detection of the unsaturated iron carbonyl species have been made. The approaches include chemical trapping [14,26], VUV induced LIF detection of CO fragments [28] and the mass spectrometry detection of unsaturated iron carbonyl [29]. Measurements of product distributions in these experiments were convoluted by e.g., the collision effects in chemical trapping, secondary fragmentation following ionization in mass spectrometry, and dependence on the modeling. Direct detection of $Fe(CO)_n$ fragments was performed by Weitz and coworkers [30] with gas-phase IR absorption spectra on the ns-μs time scale. The UED technique detects the products in a direct manner and is capable of providing product distributions and elucidating molecular structures of the isolated gas-phase reaction.

For a starting point, we assumed first that just one product was generated in the reaction. The fraction and the structural parameters were fitted iteratively in least-square manner to give the best agreement between theoretical and experimental $\Delta sM(s)$ curves [34,35]. In the fitting, the structural symmetry of each fragment was kept fixed (see Fig. 2). The Fe–C and C–O distances were taken as initial parameters similar to the parent (1.82 Å and 1.16 Å, respectively), but refined later for all the products ($Fe(CO)_x$, $x = 4, 3, 2, 1$). For the angles and symmetries of the species, we used the IR and theoretical data [22–25].

Fig. 4 shows the best fits with each assumed product. The fits with $Fe(CO)_4$ and $Fe(CO)_3$ are unacceptable while those with $Fe(CO)_2$, Fe(CO) and Fe are clearly converging. This implies that the fraction of $Fe(CO)_4$ and $Fe(CO)_3$ structures are relatively small in the reaction product whereas those of $Fe(CO)_2$, Fe(CO) and Fe are significant. Based on the energetics of the total available energy and the binding energies [20,28], the results are consistent with the two photon energy; at one photon excitation, only $Fe(CO)_4$ and $Fe(CO)_3$ are expected. A fitting with six components ($Fe(CO)_n$, $n = 0–5$) was also made by floating the fraction of each species and using the fixed structural parameters obtained from IR and ab initio calculations. The results are consistent with the single component trials, where the concentration of $Fe(CO)_5$ and $Fe(CO)_4$ are less than 0.1%.

For structural and product distribution analysis, we incorporated the three major products of the reaction, $Fe(CO)_2$, Fe(CO) and Fe. In the fitting, the mean amplitudes of vibration of intermediates were kept fixed at the same value as those of the parent. Fig. 5 shows the result of this fit. The fractions were 2% (±1%), 5% (±2%) and 5% (±1%) for $Fe(CO)_2$, Fe(CO) and Fe, respectively, indicating that 12% of the total parent $Fe(CO)_5$ molecules in the molecular beam dissociated into these products.

An interesting aspect of our results is the fitted structural parameters of $Fe(CO)_2$ and Fe(CO). The C–O bond distance is increased from 1.15 Å in $Fe(CO)_5$ to 1.34 Å (±0.10). This indicates that the C–O becomes a weaker bond in the transient fragment. The results are consistent with the finding obtained from IR studies of matrix-isolated iron carbonyls [25]. The IR C–O stretching frequencies of $Fe(CO)_2$ and Fe(CO) were found to be smaller than those of $Fe(CO)_5$, $Fe(CO)_4$ and $Fe(CO)_3$. However, our C–O distance 1.20 Å (±0.16) in Fe(CO) does not appear to scale (decreasing its strength) with the number of CO's around Fe. The trends in Fe–C

distances in $Fe(CO)_2$ and Fe(CO) are noteworthy (1.67 ± 0.25 Å and 1.78 ± 0.32 Å), but the margin of the error is larger; the errors are one standard deviations of the fitting parameters and do not account for any systematic errors.

In the conventional model describing the bonding between a transition-metal atom and a carbon monoxide with σ-bonding and π-back bonding [10,11], CO donates its filled weakly antibonding 5σ orbital to the metal orbital, strengthening the C–O bond. The metal may back-donate a filled d orbital into the empty $2\pi^*$ orbital of CO, thereby weakening the C–O bond. As noted before [11,25], increased π-back bonding is apparently more important than increased σ-bonding in $Fe(CO)_2$ and Fe(CO). More accurate analysis of structural changes demands better signal-to-noise ratio, which is the focus of ongoing project in our laboratory; extension of the *s*-range and the increase of the total pulse energy are two improvements for the next study of this and other reactions. We also plan further experiments at different energies to map out the onset of different reaction channels.

For UED with the temporal diffraction-difference method, it is clear that the sensitivity to structural changes and products distribution is now at a new level, promising extensions to many other systems and studies. With ps and sub-ps resolution the UED

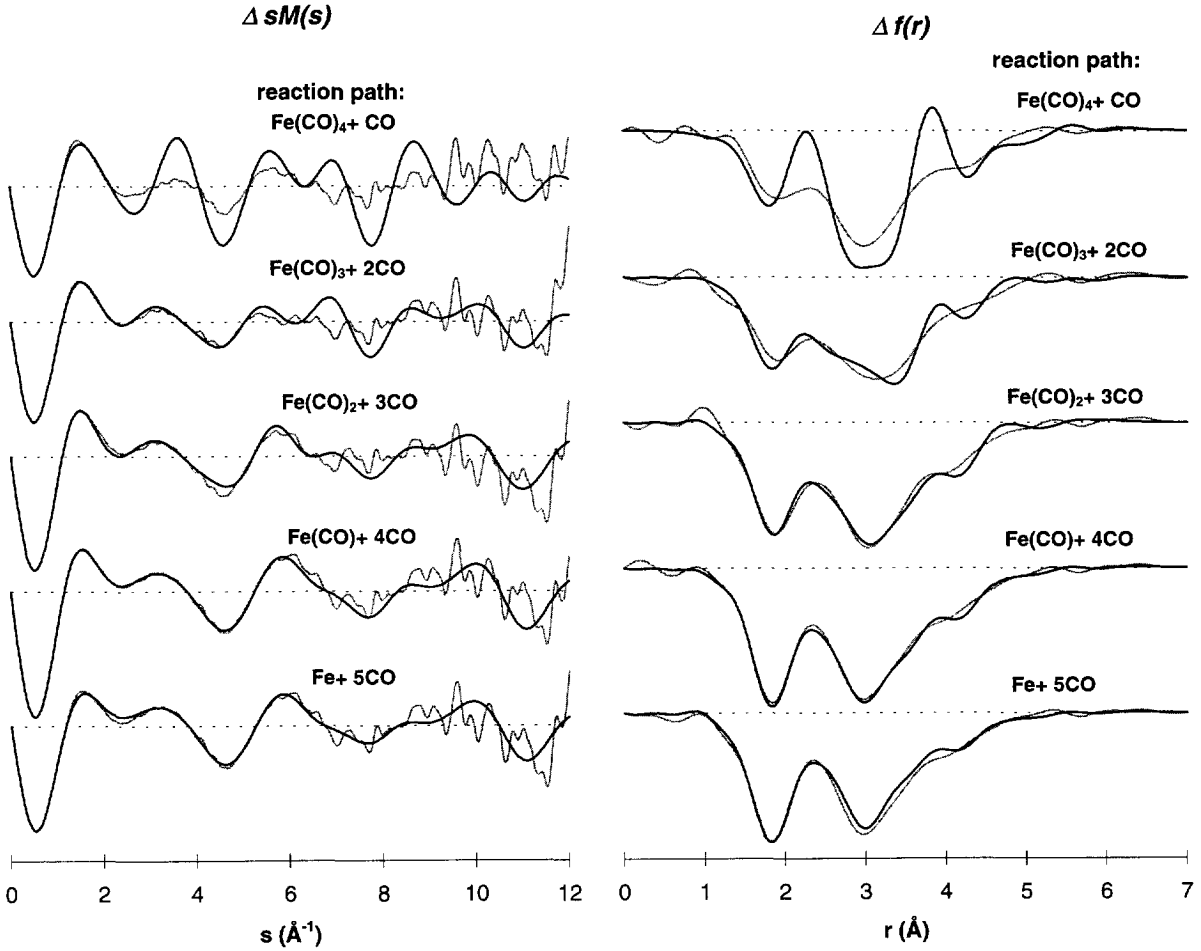

Fig. 4. Diffraction-difference modified molecular scattering curves (left) and radial distribution curves (right) obtained by fitting a one-component product distribution. Shaded lines are experimental curves and solid lines are the theoretical fits.

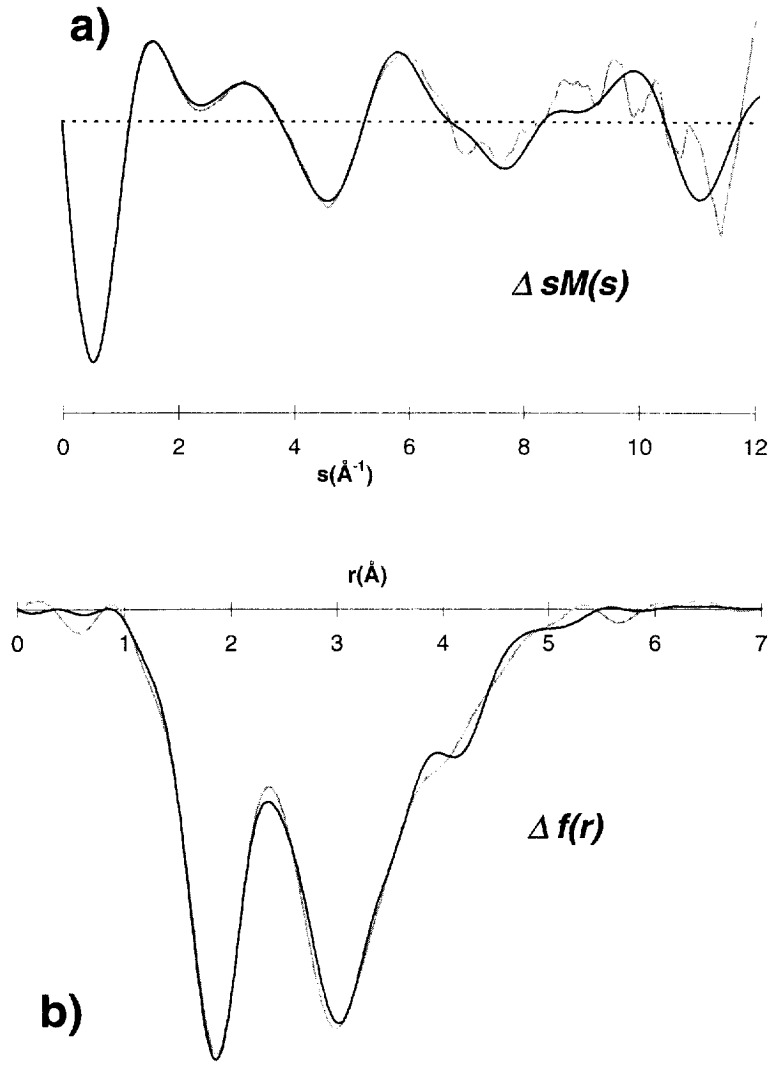

Fig. 5. Best fits obtained for product distributions of $Fe(CO)_2$, Fe(CO) and Fe. (a) The diffraction-difference modified molecular scattering curve and (b) the diffraction-difference radial distribution curve. Shaded lines are experimental curves and solid lines are the theoretical fits.

is reaching the percentage change and structural sensitivity reported using X-ray crystallography on the time scale of nanoseconds [8].

Acknowledgements

This work was supported by a grant from the Airforce Office of Scientific Research, the Office of Naval Research and the Laboratory for Molecular Sciences. We thank Chuck Williamson for his interest and initial efforts.

References

[1] J.C. Williamson, J. Cao, H. Ihee, H. Frey, A.H. Zewail, Nature 386 (1997) 159, and references therein.
[2] M. Dantus, S.B. Kim, J.C. Williamson, A.H. Zewail, J. Phys. Chem. 98 (1994) 2782, see also preceding paper.
[3] I. Hargittai, M. Hargittai (Eds.), Stereochemical Applications Of Gas-Phase Electron Diffraction. VCH, New York, 1988, and references therein.
[4] A.A. Ischenko, L. Schäfer, J.Y. Luo, J.D. Ewbank, J. Phys. Chem. 98 (1994) 8673.
[5] H.E. Elsayed-Ali, Proc. SPIE 2521 (1995) 92.
[6] F. Ráksi, K.R. Wilson, Z. Jiang, A. Ikhlef, C.Y. Côté, J.-C. Kieffer, J. Chem. Phys. 104 (1996) 6066.

[7] R.W. Schoenlein, W.P. Leemans, A.H. Chin, P. Volfbeyn, T.E. Glover, P. Balling, M. Zolotorev, K.-J. Kim, S. Chattopadhyay, C.V. Shank, Science 274 (1996) 236.
[8] V. Šrajer, T. Teng, T. Ursby, C. Pradervand, Z. Ren, S. Adachi, W. Schildkamp, D. Bourgeois, M. Wulff, K. Moffat, Science 274 (1996) 1726.
[9] I.V. Tomov, P. Chen, P.M. Rentzepis, J. Appl. Cryst. 28 (1995) 358.
[10] G.L. Geoffroy, M.S. Wrighton, Organometallic Photochemistry, Academic Press, New York, 1979.
[11] G.A. Ozin, A.J. Hanlan, Inorg. Chem. 18 (1979) 2091.
[12] I. Wender, P. Pino, Organic Synthesis via Metal Carbonyls, Vols. 1 and 2, Wiley, New York, 1977.
[13] M.S. Wrighton, D.S. Ginley, M.A. Schroeder, D.L. Morse, Pure Appl. Chem. 41 (1975) 671.
[14] G. Nathanson, B. Gitlin, A.M. Rosan, J.T. Yardley, J. Chem. Phys. 74 (1981) 361.
[15] M. Kotzian, N. Rösch, H. Schröder, M.C. Zerner, J. Am. Chem. Soc. 111 (1989) 7687.
[16] C.E. Housecroft, K. Wade, B.C. Smith, J. Organomet. Chem. 170 (1979) C1.
[17] D. Guenzburger, E.M.B. Saitovitch, M.A. De Paoli, H. Manela, J. Chem. Phys. 80 (1984) 735.
[18] J. Li, G. Schreckenbach, T. Ziegler, J. Am. Chem. Soc. 117 (1995) 486.
[19] P.C. Engelking, W.C. Lineberger, J. Am. Chem. Soc. 101 (1979) 5569.
[20] K.E. Lewis, D.M. Golden, G.P. Smith, J. Am. Chem. Soc. 106 (1984) 3905.
[21] B. Beagley, D.G. Schmidling, J. Mol. Struct. 22 (1974) 466, and references therein to earlier work.
[22] L.A. Barnes, M. Rosi, C.W. Bauschlicher Jr., J. Chem. Phys. 94 (1991) 2031.
[23] M. Poliakoff, J.J. Turner, J. Chem. Soc. Dalton Trans. (1974) 2276.
[24] M. Poliakoff, J. Chem. Soc. Dalton Trans. (1974) 210.
[25] C.H.F. Peden, S.F. Parker, P.H. Barrett, R.G. Pearson, J. Phys. Chem. 87 (1983) 2329.
[26] J.T. Yardley, B. Gitlin, G. Nathanson, A.M. Rosan, J. Chem. Phys. 74 (1981) 370.
[27] R.L. Whetten, K.-J. Fu, E.R. Grant, J. Chem. Phys. 79 (1983) 4899.
[28] I.M. Waller, J.W. Hepburn, J. Chem. Phys. 88 (1988) 6658.
[29] U. Ray, S.L. Brandow, G. Bandukwalla, B.K. Venkataraman, Z. Zhang, M. Vernon, J. Chem. Phys. 89 (1988) 4092.
[30] E. Weitz, J. Phys. Chem. 98 (1994) 11256, and references therein.
[31] S.K. Kim, S. Pedersen, A.H. Zewail, Chem. Phys. Lett. 233 (1995) 500.
[32] L. Bañares, T. Baumert, M. Bergt, B. Kiefer, G. Gerber, Chem. Phys. Lett. 267 (1997) 141.
[33] L. Schäfer, Appl. Spectrosc. 30 (1976) 123.
[34] K. Hedberg, M. Iwasaki, Acta. Cryst. 17 (1964) 529.
[35] L.S. Bartell, in: A. Weissbergre, B.W. Rossiter (Eds.), Physical Methods of Chemistry, Wiley, New York, 1972.